

Trace level detection and identification of nitro-based explosives by surface-enhanced Raman spectroscopy

S. Botti,* S. Almaviva, L. Cantarini, A. Palucci, A. Puiu and A. Rufoloni

Methods for rapid identification of explosives and their associated compounds at trace level quantities are needed for security screening applications. In this paper, we apply the surface-enhanced Raman spectroscopy (SERS) to detect and identify traces (as low as tens of pg) of pentaerythritol tetranitrate (PETN), ethylene glycol dinitrate (EGDN), cyclotrimethylene-trinitramine (RDX) and trinitrotoluene (TNT) using commercially available substrates (Klarite[®], Renishaw diagnostics). High quality spectra were achieved within 10 s with a compact Raman spectrometer. Principal component analysis (PCA) of the data was performed to understand what factors affected the spectral variation across the samples. It was found that 76% of the spectral variation was explained by the first three PCs. Score plots for these components showed that the energetic materials can be clearly classified on the basis of SERS spectra also at trace level quantity. Our measurements further demonstrate the potential for using SERS as fast, *in situ* analytical tool for safety devices, with a sensitivity which competes and, in some cases, overcomes other techniques. Copyright © 2013 John Wiley & Sons, Ltd.

Keywords: SERS; trace evidence; explosives; Raman spectroscopy

Introduction

The trace level detection of explosive compounds is a rapidly evolving field of crucial interest for environmental safety and homeland security. In this frame, the surface-enhanced Raman spectroscopy (SERS), has gained increasing importance because, since its first observation,^[1,2] the surface enhancement effect promised to overcome the problems arising from the low sensitivity of Raman spectroscopy, combining its analytical advantages with the possibility of trace level detection. The surface enhancement effect was explored actively either to give a deeper insight in its origin or to assess its usefulness for a safety device.^[3–9]

It is commonly accepted that two major types of mechanisms contribute to the surface enhancement: an electromagnetic effect, due to the large optical fields generated near the surface by electromagnetic resonances between the collective oscillations of plasmons in metal particles and the incident optical field, and a chemical one related to an increased polarisability of the adsorbed molecule due to the coupling with the metal surface. In principle, all the metals should display the surface enhancement, but, in practice, it was observed that the Raman scattering signal is strongly amplified only when the molecule is adsorbed on a coinage metal substrate, and this effect is maximised when the localised surface plasmon resonance frequency coincides with that of the excitation laser.

The in-field applications of SERS depend on the availability of compact Raman platforms with high sensitivity and of robust substrates, which can guarantee the adequate enhancement factor, that could be integrated in a SERS probe permitting a rapid *in situ* detection and screening. To this respect, the aim of the present work is to explore the possibility to use SERS, performed with compact Raman platform, to detect and identify quantity as low as tens of pg of nitro-based explosive compounds. We

measured the surface-enhanced Raman signal from controlled quantities of explosive molecules deposited on industrially made nanostructured substrates, and, due to the high enhancement factor of the surface, high quality Raman spectra were recorded with acquisition times of 10 s. Principal component analysis (PCA) of the data was performed to understand what factors affected the spectral variation across the samples.

Our results, discussed in the following, validate the use of the SERS technique, also with lower cost compact Raman platform, for in-field security diagnostics.

Experimental

Spectroscopic instrumentation

The Raman spectra were acquired with an integrated Raman system (BWTEK inc., *i*-Raman), in the wavelength range 789–1048 nm corresponding to Raman shifts of 75–3200 cm⁻¹ (resolution 3 cm⁻¹). The excitation source was a solid state laser with 785 nm light and a power scalable in the range 30–300 mW. The near-IR excitation eliminates most of sample fluorescence. The Raman system is equipped with a micropositioning system for fine xyz adjustments and a video camera for sampling viewing. Depending on the mounted microscope objectives, the laser has a diameter of 180 μm, 90 μm or 50 μm.

* Correspondence to: S. Botti, ENEA, UTAPRAD, Via Enrico Fermi 45, 00044 Frascati, Italy. E-mail: Sabina.Botti@enea.it

ENEA UTAPRAD Via Enrico Fermi 45, 00044 Frascati, Italy

To analyse the spectroscopic data, we performed the PCA with a program developed in the MatLab platform which uses the correlation matrix described in details elsewhere.^[10]

PCA is a widely used technique for data classification and gives as result the PCs which contain information about changes in the spectral features of the Raman spectra across the samples. By plotting the scores of the PCs, which represent the largest variance within the data set, against each other, a plot in which each sample is represented by a point can be generated. It is expected that in this plot, the samples that are closely related are grouped together, whereas unrelated samples are observed as outliers.

Samples

To prepare the samples, we used the following commercially available solution: pentaerythritol tetranitrate (PETN) in methanol (Superchrom, 1 mg/ml, 100 µg/ml), ethylene glycol dinitrate (EGDN) in methanol (Sigma, 1 mg/ml, 100 µg/ml), cyclotrimethylene-trinitramine (RDX) in methanol/acetonitrile (Superchrom, 1 mg/ml, 100 µg/ml) and trinitrotoluene (TNT) in methanol/acetonitrile (Sigma, 1 mg/ml, 100 µg/ml).

A controlled volume of solution was dropped on the substrate. The solvent selectively evaporates leaving the dried molecule adsorbed on the surface, Raman measurements can be carried out across the deposited patch, clearly visible under the optical microscope coupled with the spectrometer. In our procedure, the substrate was used as received without any pre-treatment and the solvent evaporated in the air.

The evaporation process of any liquid on a surface produces different patches that depend on the interplay of adhesive forces of the substrate and cohesive forces of the fluid. Usually, crystalline islands inside the patch are not formed because we used diluted solutions (10^{-3} M, 10^{-4} M) that leave a uniform layer. Therefore, the quantity probed by the laser can be estimated as the analyte dropped mass multiplied by the ratio between the laser spot and the patch area. As already mentioned, the area sampled by the laser depends on the microscope objective through which the laser is focused. For the present measurements, a laser spot of 90 µm diameter was used (objective 20×). Because the area of the deposited patch, evaluated through optical microscope observations, resulted to be of some mm², the analyte mass in the laser beam is typically one thousandth of that deposited. As an example, a drop of 0.1 µl at a concentration of 100 µg/ml, expanding over an

area of 5 mm², corresponds to about 13 pg of analyte detected in the laser beam area of $6.4 \cdot 10^{-3}$ mm².

In our SERS experiments, we used substrates fabricated by depositing a gold layer on a silicon surface with an ordered nanostructure produced by microlithography (Klarite[®], Renishaw diagnostics). The enhancement effect of these substrates was already demonstrated,^[11–14] in particular, the regularity of their nanostructure guarantees a high reproducibility of Raman signal coming from different parts of the same surface as requested for analytical applications. The SERS substrate morphology was examined under high-resolution electron microscope (HRSEM), using a Leo 1525 hot cathode field emission microscope, with a resolution of 1.5 nm at 20 kV.

Results and discussion

In our SERS experiments, we used gold-coated (100) oriented Si substrates. The surface consists of a lattice of inverted square-based pyramids with a fixed apex pit angle of 70.5° and a pit aperture aligned along the (111) directions of the Si wafer (see Fig. 1). The gold layer deposited onto the internal walls of the pyramids has a nanostructured roughness with a feature size of about 20 nm. The theoretical models assume^[15,16] that the surface plasmons excited on the gold film surface were reflected by the top convex sharp pit edge, then oscillated backward and forward along the faces of each pyramid and interfered with themselves in the cavity, producing a standing wave which localises the plasmons with consequent Raman signal amplification when the molecules, or portion of them, occupy the pyramid faces. Three-dimensional numerical simulations revealed that the contribution of diffraction effects to surface enhancement in the Klarite structure is noticeable for gold coating thickness larger than 125 nm.^[17]

It was demonstrated that plasmonic energies depend on the pit dimension *L*. In our previous work^[12] we used Klarite[®] substrates with *L* = 1.5 µm, whereas in the present work, the void aperture size is much smaller (about 500 nm) and a higher surface enhancement factor is expected.

To compare with the Raman scattering without surface enhancement, we deposited the explosive solution also on the non active part of the gold surface, without the array of pyramidal pits. When we dropped in this substrate portion, the same volume of explosive solution as the one used in the SERS experiments, no Raman signal could be detected. Because, with the HRSEM, we verified that the

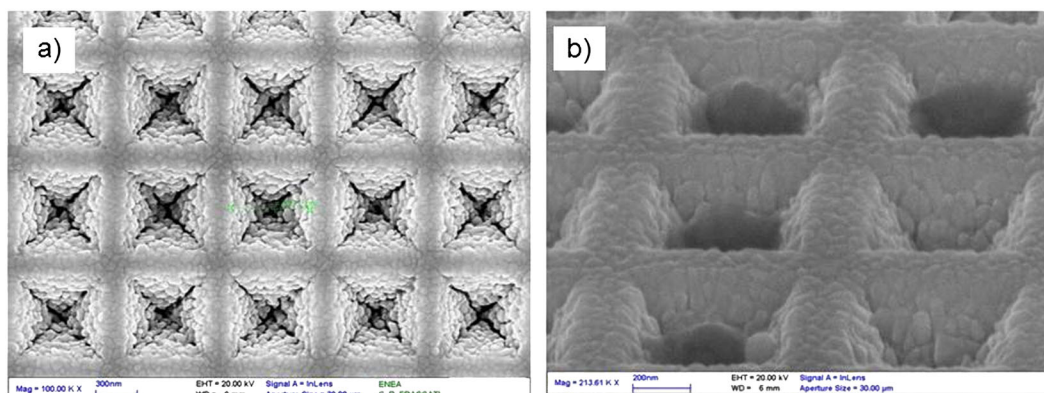


Figure 1. HR-SEM images of Klarite SERS substrate surface: (a) square-based pyramidal pits array aligned on the Si (100) direction; (b) tilted view of inverted pyramids.

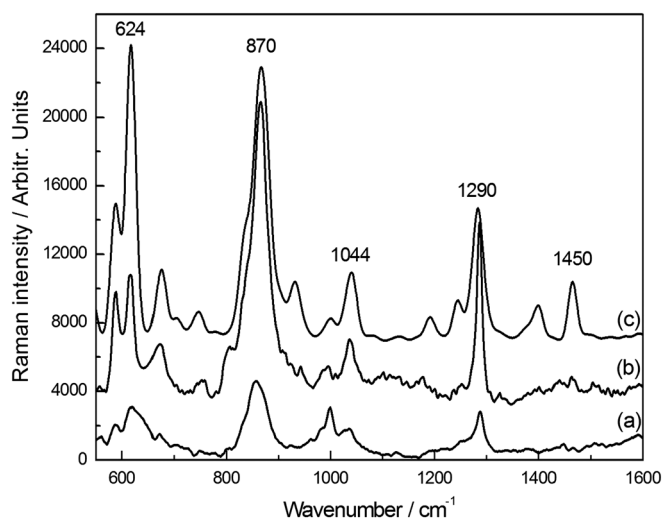


Figure 2. SERS spectra of PETN: the estimated quantities probed by laser are 5 pg (curve a) and 200 pg (curve b). Curve c: Raman trace acquired from 0.2 μg of PETN. All the spectra are accumulated for 10 s and are reported at the same scale, offset for clarity.

gold coating has a comparable nanoscaled structure on the pit faces and on the flat regions, this finding further confirm that the enhancement effect is due to the plasmon localisation in the pits. Therefore, to measure the 'normal' Raman spectra, it was necessary to deposit a larger quantity of sample on the substrate.

During the detection process, all the parameters were kept unchanged for a closer comparison between the experimental runs. We acquired the Raman spectra for different spatial positions across the substrate with a laser power of 180 mW focused with a 20 \times objective.

In Fig. 2, the conventional and surface-enhanced Raman spectra of 5 pg (curve a), 200 pg (curve b) and 0.2 μg of PETN (curve c) are reported. The measured Raman lines match well with literature data^[18–20] and can be attributed to the vibrational modes of PETN, namely 624 cm^{-1} (ONO_2 rock), 870 cm^{-1} (O–N stretching mode),

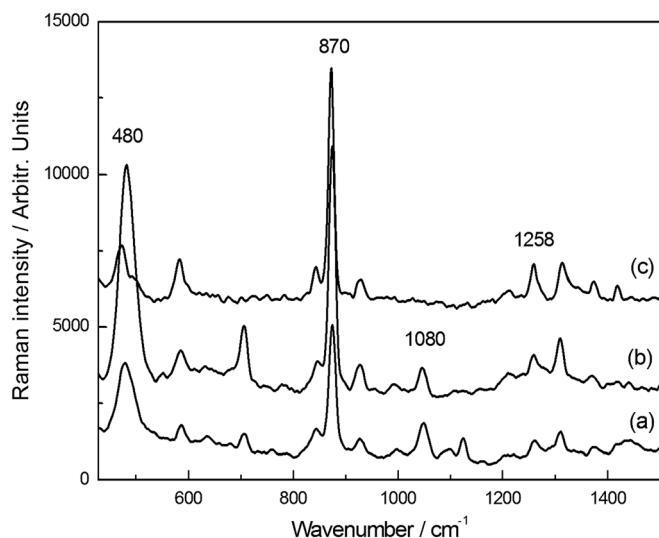


Figure 3. Surface-enhanced and conventional Raman spectra of RDX (offset for clarity, same scale). The spectra were obtained from a probed mass of: 80 pg (curve a), 200 pg (curve b), 3 μg (curve c). Integration time: 10 s.

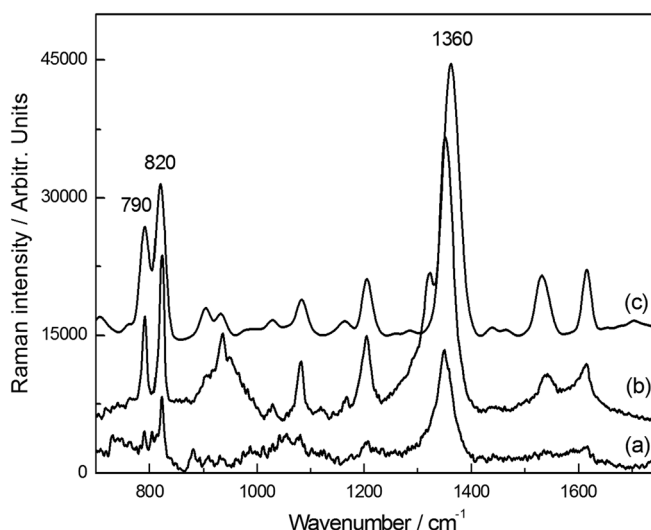


Figure 4. Raman spectra of TNT, accumulation time 10 s. Curve a: surface-enhanced Raman spectrum acquired from 20 pg; curve b: surface-enhanced Raman spectrum acquired from 200 pg; curve c: Raman spectrum acquired from 0.8 μg .

1044 cm^{-1} (CH_2 torsion and C–C bending), 1290 cm^{-1} (NO_2 symmetric stretching) and 1450 cm^{-1} (NO_2 asymmetric stretching).

Klarite[®] substrates were used also to investigate the detection of RDX at different quantities, as shown in Fig. 3. The characteristic RDX bands^[18,19,21] at 480 cm^{-1} (in plane ring bending), 870 cm^{-1} (C–N–C ring breathing mode), 1080 cm^{-1} (C–H ring in plane bend) and 1258 cm^{-1} (CH_2 scissoring, N–N stretching vibration), are also present in the SERS spectra down to a probed mass as low as 80 pg.

In Fig. 4, the spectra acquired from 20 pg (curve a), 200 pg (curve b) and 0.8 μg (curve c) of TNT are shown. The dominant feature of TNT molecule is the symmetric NO_2 stretching vibrations, observed at 1360 cm^{-1} .^[18,19,22,23] Because this mode, in combination with the bands at 790 cm^{-1} and 820 cm^{-1} (NO_2 scissoring modes), is also present in the SERS spectrum of 20 pg of TNT, this molecule can be clearly identified.

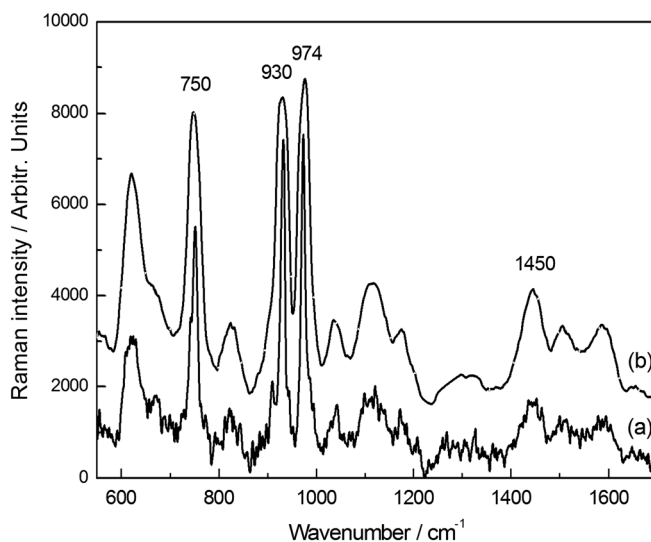


Figure 5. Curve a: surface-enhanced Raman spectrum acquired from 30 pg of EGDN; curve b: Raman spectrum acquired from 1 μg of EGDN. Both spectra were accumulated for 10 s.

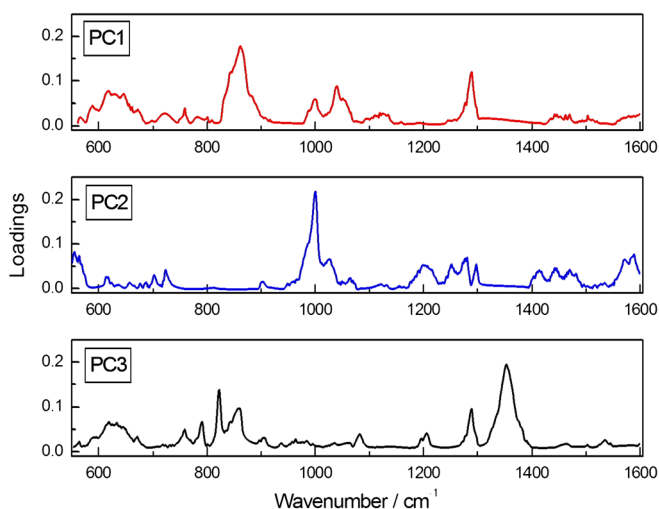


Figure 6. Loading plots for the first three components. Same scale for all plots.

The surface-enhanced Raman spectrum of 30 pg of EGDN is displayed in Fig. 5 (curve a) with the Raman spectrum of 1 μg of EGDN (curve b), as comparison. They both show large differences respect to those of PETN, although EGDN and PETN both belong to the nitrate ester class in which a NO_2 group is bound to the alkyl chain through an oxygen atom. The EGDN spectra are dominated by the intense bands of ONO_2 umbrella (750 cm^{-1}), CH_2 rock (930 cm^{-1}) and CO stretching (974 cm^{-1}), and only the asymmetric stretching of NO_2 is present^[18,19] (1450 cm^{-1}), whereas the PETN Raman traces exhibit the sharp peak at 1290 cm^{-1} of NO_2 symmetric stretching.

The observed variations in the SERS spectra across the samples play a critical role in the ability to discriminate and identify

between the nitro-based explosive compounds. We expect that explosive identification methods based on SERS spectra should exhibit enhanced specificity, as well as sensitivity at trace level. However, since only the modes of analyte moieties adsorbed on the nanostructured surfaces are strongly enhanced, when the analyte mass decreases down to few tens of pg, there are typically fewer peaks in the SERS spectrum, and this oversimplification of Raman trace could be detrimental for the correct identification of analyte.

We used PCA to identify which are the factors that mainly affect the spectral variation across the different nitro-based samples.

All the spectra were normalised to their maximum value, the spectral background was removed, and the spectra were truncated in the $550\text{--}1600\text{ cm}^{-1}$ region which contains all the relevant vibrational features, thus avoiding that small and non relevant bands can acquire the same importance as the large bands related to important functional groups. In this way, a data matrix of 67 samples and 536 data points was constructed to be submitted to the PCA algorithm.

PCA shows that retaining only the first three PCs explains the 76% of the overall spectral variation. The corresponding loading plots, which indicate the specific contribution of each vibrational bands in the total variance of spectral data, are reported in Fig. 6.

The first PC, PC1, which accounts for the 39.4% of spectral variance, has two main peaks that correspond to the overlapping of C–N–C ring breathing and O–N stretching region and to the NO_2 symmetric stretching vibration in nitrate ester, respectively. In the second component, PC2, with an explained spectral variance of 23.2%, the peak features correspond to the CH_2 rocking and CO stretching. The loading plot for PC3, which explains the 13.3% of spectral variance, shows, besides smaller peaks in position equivalent to those in the PC1 loading plot, a strong band in the NO_2 symmetric stretching position (1360 cm^{-1}). The low PC coverage is in agreement with the large spectral differences between the SERS spectra.

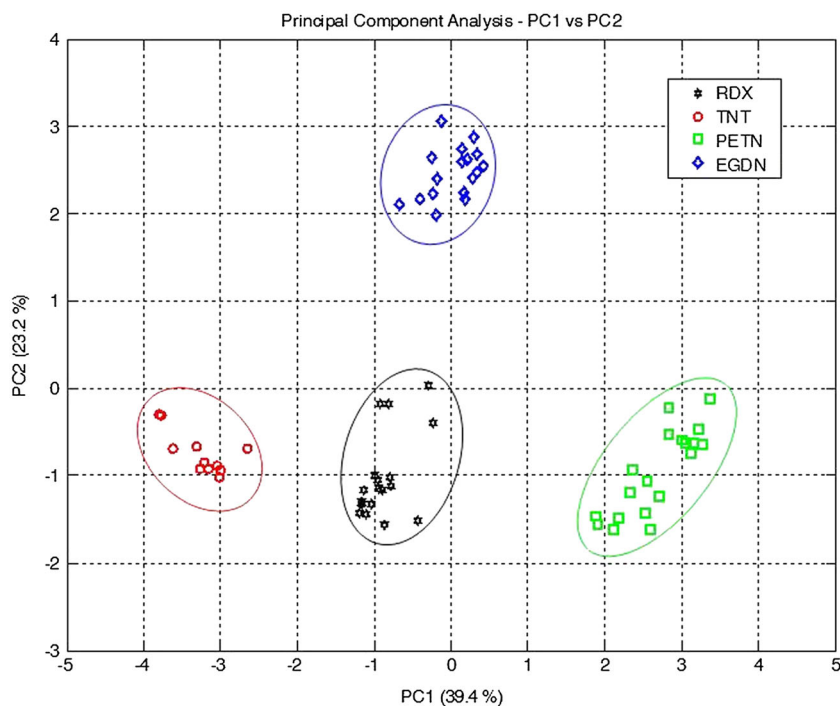


Figure 7. A PCA 2D score plot of PC1 versus PC2 for the SERS and Raman spectra dataset. Numbers in parentheses on each axis represent the percentage variance that each principal component accounts for.

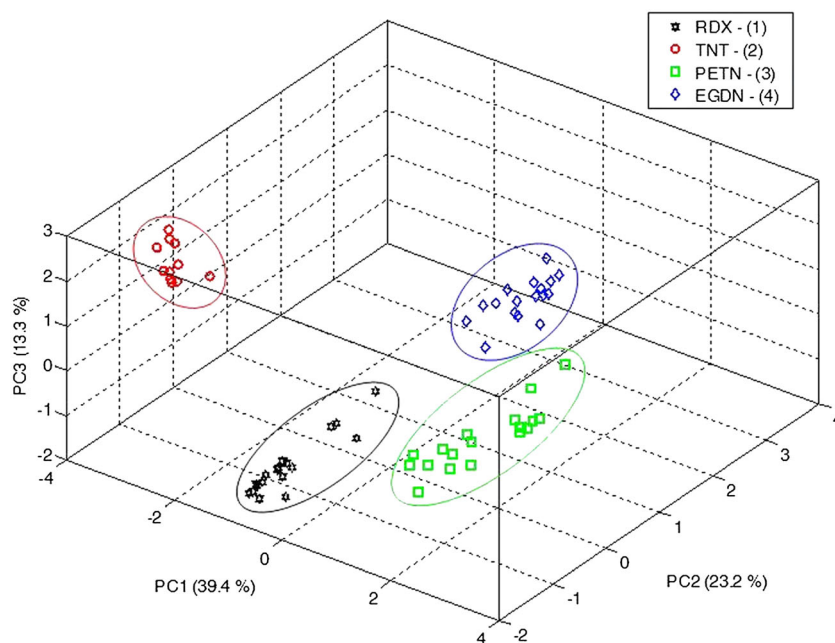


Figure 8. A PCA 3D score plot of PC1 versus PC2 versus PC3 for the SERS and Raman spectra dataset. Numbers in parentheses on each axis represent the percentage variance that each principal component explains.

Only two components can be sufficient to describe the data set, as evidenced in Fig. 7, which shows the PCA plot for the PC1 and PC2, the two largest PCs of the dataset, which explain 62.6% of the spectral variance between the samples. In this plot, each sample is represented by a point, and the four groups, each corresponding to an explosive compound, are clearly separated.

In Fig. 8, we report the 3D plot of PC1, PC2 and PC3 (76% explained variance), which clearly shows that each compound can be correctly grouped with no miss assignment. Therefore, the application of PCA to the Raman spectra expressed by 536 different wavelengths has allowed to reduce the output to only three components.

The score plots indicate that the proposed model is able to correctly group the nitro-based compounds, and, we have shown that we are able to identify explosive compounds at tens of pg level, in spite of the oversimplification of SERS spectra (these samples are represented by the points in the outer region of each group).

Currently, the largest limitation of the model is the number of chemical species in the dataset; however, this is an important first step to demonstrate that the rapid identification of explosive compounds at trace level is routinely possible with SERS technique also using a compact Raman platform.

Conclusions

In summary, we performed surface-enhanced and conventional Raman spectroscopy on explosive molecules by using compact, portable Raman instrument and commercially available substrates. Spectra suitable for molecular identification were accumulated in only 10 s. Explosive compounds were detected and identified at trace level quantities, as low as tens of pg.

Applying PCA to the SERS spectra, it was found that 76% of the spectral variation was accounted for by the first three PCs. As expected from the large spectral differences, exemplified by the low PC coverage, analysis of the score and loading plots for these components showed that the samples can be clearly classified on

the basis of vibrational modes of functional groups, with no miss assignment. Our measurements further indicate the enhanced specificity as well as sensitivity obtained from the SERS approach with respect to other techniques and strongly support the possible effectiveness of using SERS in a practical detection instrument for security diagnostics.

Acknowledgements

We acknowledge the financial support of the EC in the framework of the BONAS project (FP7-SEC-2010-1).

References

- [1] D. L. Jeanmaire, R. P. Van Duyne, *J. Electroanal. Chem.* **1977**, *84*, 1.
- [2] C. L. Haynes, A. D. McFarland, R. P. Van Duyne, *Anal. Chem.* **2005**, *77*, 339, and references therein.
- [3] K. Kneipp, Y. Wang, R. R. Dasari, M. S. Feld, B. D. Gilbert, J. Janni, J. I. Steinfeld, *Spectrochimica acta part A*, **1995**, *51*, 2171.
- [4] D. S. Moore, *Rev. Sci. Instrum.*, **2004**, *75*, 2499.
- [5] K. Kneipp, H. Kneipp, I. Itskan, R. R. Dasari, M. S. Feld, *Chem. Rev.*, **1999**, *99*, 2957.
- [6] K. Kneipp, Y. Wang, H. Kneipp, L. T. Perelman, I. Itzkan, R. R. Dasari, M. S. Feld, *Phys. Rev. Lett.*, **1997**, *78*, 1667.
- [7] S. Nie, S. R. Emory, *Science*, **1997**, *27*, 1102.
- [8] J. M. Silvia, J. A. Janni, J. D. Klein, K. M. Spencer, *Anal. Chem.*, **2000**, *72*, 5834.
- [9] H. Wackerbarth, L. Gundrum, C. Salb, K. Christou, W. Viol, *Appl. Opt.*, **2010**, *49*(23), 4367.
- [10] G. Giubileo, F. Colao, A. Puiu, *Laser Physics*, **2012**, *22*(6), 1033.
- [11] X. Fang, S. R. Ahmad, *Appl. Phys. B*, **2009**, *97*, 723.
- [12] S. Botti, L. Cantarini, A. Palucci, *J. Raman Spectrosc.*, **2010**, *41*, 866.
- [13] F. H. Scholes, T. J. Davis, K. C. Vernon, D. Lau, S. A. Furman, A. M. Glenn, *J. Raman Spectrosc.*, **2012**, *43*, 196.
- [14] J. Li, X. Xu, Y. Wang, M. Wang, Z. Dong, W. Tian, J. Sun, C. Zhang, B. Wang, *J. Raman Spectrosc.*, **2012**, *43*, 863.
- [15] N. M. B. Perney, J. J. Baumberg, M. E. Zoorob, M. D. B. Charlton, S. Mahnkopf, M. C. Nett, *Opt. Express*, **2006**, *14*(2), 847.
- [16] N. M. B. Perney, F. J. de Abajo, J. J. Baumberg, A. Tang, M. C. Nett, M. D. B. Charlton, M. E. Zoorob, *Phys. Rev. B*, **2007**, *76*, 035426.

- [17] K. C. Vernon, T. J. Davis, F. H. Scholes, D. E. Gomez, D. Lau, J. Raman *Spectrosc.*, **2010**, *41*, 1106.
- [18] I. R. Lewis, N. W. Daniel Jr, P. R. Griffiths, *Appl. Spectroscopy*, **1997**, *51*, 1854.
- [19] N. W. Daniel Jr, I. R. Lewis, P. R. Griffiths, *Appl. Spectroscopy*, **1997**, *51*, 1868.
- [20] Y. A. Gruzdkov, Y. M. Gupta, *J. Phys. Chem. A*, **2001**, *105*, 6197.
- [21] N. A. Hatab, G. Eres, P. B. Hatzinger, B. Gu, J. Raman, *Spectrosc.*, **2010**, *41*, 1131.
- [22] R. H. Clarke, S. Londhe, W. R. Premasiri, M. E. Womble, *J. Raman Spectrosc.*, **1999**, *3*, 827.
- [23] M. R. Lewis, I. R. Lewis, P. R. Griffiths, *Vibrational Spectroscopy*, **2005**, *38*, 11.